Terra MODIS On-Orbit Spatial Characterization and Performance

Xiaoxiong Xiong, Nianzeng Che, and William Barnes

***Abstract*—The Moderate Resolution Imaging Spectroradiometer (MODIS) Proto-Flight Model, onboard the National Aeronautics and Space Administration's Earth Observing System Terra spacecraft, has been in operation for over four years. It has 36 spectral bands and a total of 490 detectors located on four focal plane assemblies (FPAs). MODIS makes observations at three spatial resolutions (nadir): 0.25 km (bands 1–2), 0.5 km (bands 3–7), and 1 km (bands 8–36). The instrument's spatial characterization was measured prelaunch using an integration and alignment collimator. Parameters measured included the detectors' instantaneous field-of-view (IFOV), band-to-band registration (BBR), and line spread function in both the along-scan and along-track directions. On-orbit, the spatial characterization is periodically measured using the onboard spectro-radiometric calibration assembly (SRCA). This paper describes the SRCA BBR algorithms, characterization methodologies, and on-orbit results. A Fourier approach used to calculate the along-track BBR is also described. This approach enhances the algorithm's robustness in comparison with the conventional centroid approach. On-orbit results show that the Terra MODIS focal planes shifted slightly during launch and initial on-orbit operation. Since then they have been very stable. The BBR is within 0.16 km (nadir IFOV) in the along-scan direction and 0.23 km (nadir IFOV) in the along-track direction among all bands. The small but noticeable periodic variation of the on-orbit BBR can be attributed to the annual cycling of instrument temperature due to sun–earth distance variation. The visible FPA position has the largest temperature dependence among all FPAs, 17 m/K along-scan and 0.6 m/K along-track.**

***Index Terms*—Calibration, instrument, remote sensing, spatial alignment.**

I. Introduction

THE Moderate Resolution Imaging Spectroradiometer (MODIS) Proto-Flight Model (PFM) has been operating on-orbit since its launch on December 18, 1999, providing continuous global data for studies of the earth's land, oceans, and atmosphere [1]–[3]. It has 36 spectral bands located on four focal plane assemblies (FPAs) covering wavelengths in the visible (VIS), near infrared (NIR), short- and midwave infrared (SMIR), and longwave infrared (LWIR). The SMIR and LWIR FPAs are radiatively cooled to their nominal operating temperature of 83 K. MODIS has three different nadir ground spatial resolutions: 0.25 km (bands 1–2), 0.5 km (bands 3–7), and 1 km (bands 8–36). For bands with subkilometer resolution, multiple subsamples are acquired in the along-scan direction (four for bands 1–2 and two for bands 3–7). In the along-track direction, there are 40 detectors per band for bands 1–2, 20 detectors per band for bands 3–7, and ten detectors per band for bands 8–36. MODIS bands 1–19 and 26 with wavelengths from 0.41–2.2 μm are categorized as the reflective solar bands (RSBs), and the remaining are the thermal emissive bands (TEBs) with wavelengths from 3.5–14.5 μm.

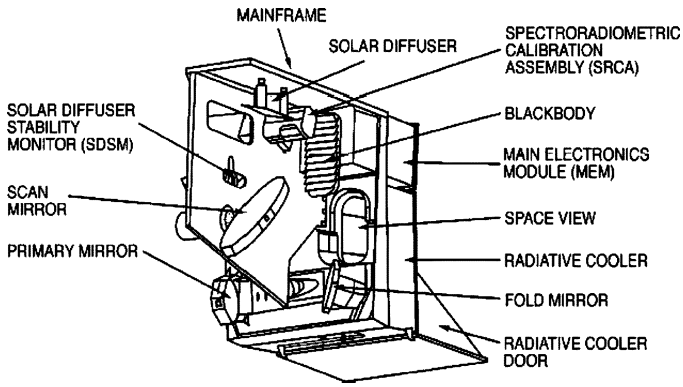

Fig. 1. MODIS instrument.

As shown in Fig. 1, MODIS uses a double-sided scan mirror that views the onboard calibrators (OBCs) and the earth scene at 20.3 r/min. It is equipped with a number of onboard calibrators: a v-grooved blackbody (BB), a solar diffuser (SD), a solar diffuser stability monitor (SDSM), a spectro-radiometric calibration assembly (SRCA), and a spaceview port (SV). They are located opposite the earth view. Hence, when the scan mirror is rotating, one side of the mirror views the earth scene, and the other side consecutively views the calibrators. The BB and SV data used for calibration of the thermal emissive bands are obtained every scan, while the SD and SDSM were operated weekly during the first year and biweekly thereafter for calibration of the reflective solar bands [4]–[6]. The SDSM is used to track SD reflectance degradation on-orbit.

The SRCA has three operational modes: spatial, spectral, and radiometric. The spatial mode, operated bimonthly, is used to track the band-to-band registration (BBR) of all 36 bands from prelaunch to on-orbit and their changes over time [7]–[9]. In spectral mode, operated trimonthly, the SRCA functions as a self-calibrated monochromator to characterize RSB spectral response and center wavelength shifts [10], [11]. The radiometric mode, typically operated monthly, is used to monitor RSB response changes at an angle of incidence (AOI) of 38.2° to the scan mirror and to support the RSB calibration by the SD (i.e., performed at an AOI to the scan mirror of 50.2°) [12].

Manuscript received May 10, 2004; revised October 13, 2004.

X. Xiong is with the Earth Sciences Directorate, NASA Goddard Space Flight Center, Greenbelt, MD 20771 USA (e-mail: xiaoxiong.xiong.1@gsfc.nasa.gov).

N. Che is with Science Systems and Applications, Inc., Lanham, MD 20706 USA (e-mail: nianzeng_che@ssaihq.com).

W. Barnes is with University of Maryland Baltimore County, Baltimore, MD 21250 USA (e-mail: wbarnes@neptune.gsfc.nasa.gov).

Digital Object Identifier 10.1109/TGRS.2004.840643

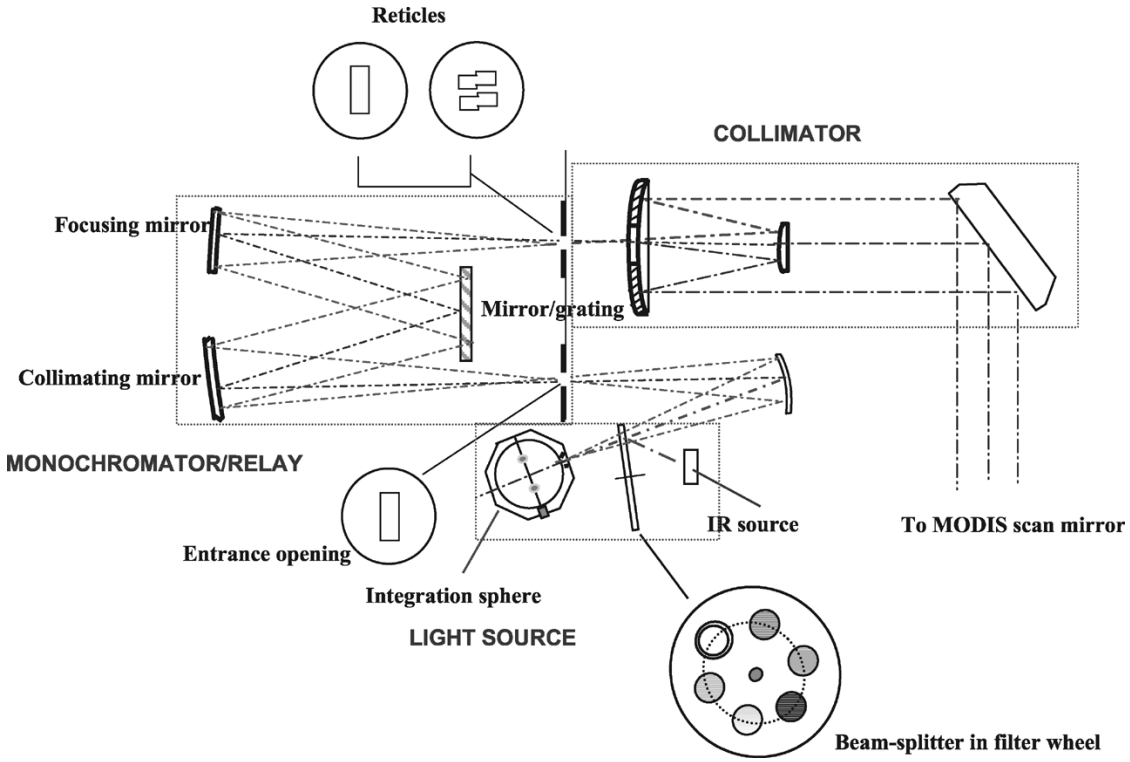

Fig. 2. Layout of the SRCA.

The SRCA contains VIS/NIR and infrared (IR) sources, a monochromator or optical relay, and a collimator (Fig. 2). The VIS/NIR source is a spherical integration source (SIS) with four 10-W lamps and two 1-W lamps (one of the 10-W lamps and one of the 1-W lamps are backups) to provide multiple levels of illumination for the RSB characterization. A thermal source provides IR energy. When the SRCA is in spatial mode, a beam-combiner on the filter wheel is used. The light coming out of the SIS passes through it while the IR beam is reflected from its surface. The combined beams provide illumination for all 36 bands. The light passes through the beam combiner and is focused onto the monochromator's entrance slit. After reflection by a collimating mirror, the beam passes onto a mirror or grating (the grating is used for the spectral characterizations). The beam is then refocused onto an exit slit (or various interchangeable reticles) by the focusing mirror. The follow-up Cassegrain telescope system expands and collimates the beam before it exits the SRCA and is viewed by the MODIS scan mirror.

When the SRCA is in spatial mode, an entrance slit equivalent to a 5 km (scan direction) $\times$12 km (track direction) nadir IFOV [Fig. 3(a)] is used. The mirror, instead of the grating, is in position so that the monochromator functions as a simple optical relay system. Located at the exit position are two reticles: one for along-scan, which is identical to the entrance slit [Fig. 3(a)], and the other for along-track [Fig. 3(b)] with stepped openings. The two reticles are positioned in turn to measure MODIS spatial response in both directions. The SRCA collimator and the MODIS optics image the reticles onto the FPAs.

In the spatial mode, the IR source is on, and the lamps inside the SIS are turned on in sequence of three 10 W, two 10 W, one 10 W, and 1 W. Each band utilizes one light-source configuration for its optimal (i.e., on-scale) signal. Since the lamps need warm-up time, both the along-scan and along-track measurements are performed at each lamp configuration before it is changed.

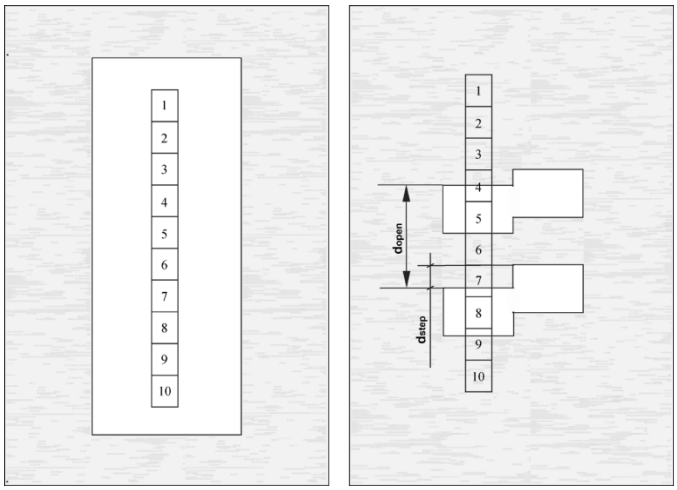

Fig. 3. SRCA spatial mode reticles (a) along-scan and (b) along-track.

II. Algorithm for Determining Along-Scan BBR

The along-scan BBR reticle images a 12-km (equivalent along-track nadir IFOV) reticle onto the FPAs. All detectors within a band are illuminated simultaneously. The knife-edge reticle cuts-on (illuminates) and then cuts-off (darkens) the detectors of each band as the scan mirror is rotated. In the along-scan direction, the 5-km IFOV width typically provides full illumination of four frames (one frame is equivalent to a 1-km nadir IFOV). Normally, MODIS takes ten frames of

SRCA data each scan. For each 1-km resolution frame, two subsamples are taken for 0.5-km resolution bands and four subsamples for 0.25-km resolution bands.

In order to improve the measurement precision, electronic phase delay of the sample timing is applied. The phase delay changes the start of data sampling time for the MODIS detectors so that the step size between two consecutive data points is reduced. The capability of phase delay can also adjust the BBR along-scan between FPA without physically shifting the FPA. The phase delay is set to have equal timing shifts so that the data sampling has delays equivalent to 0, 0.2, 0.4, 0.6, 0.8, and 1 km. The 1-km phase delay is added here for repeatability check. It produces the same results as that from the 0 phase delay with extra one frame shift and is, therefore, not used in the BBR algorithm. Including the phase delay shifts, the data sampling position in the along-scan direction x_{scan} is given by

$$x_{\text{scan}} = N_{\text{frame}} + SZ_{\text{detector}} \cdot (N_{\text{subsample}} - 1) + 0.2 \cdot N_{\text{delay}} \tag{1}$$

where

- N_{frame} frame number from 1 to 10 for the SRCA data;
- SZ_{detector} detector size as a fraction of 1-km detector size, 1/4 for bands 1–2, 1/2 for bands 3–7, and 1 for bands 8–36;
- $N_{\text{subsample}}$ subsample number from 1 through 4 for bands 1–2, 1 or 2 for bands 3–7, and 1 for bands 8–36;
- N_{delay} phase delay number from 0 to 4 corresponding to the phase delays of 0, 0.2, 0.4, 0.6, and 0.8.

For instance, the data sample position, x_{scan}, for the 0.5-km resolution bands is 1, 1.5, 2, ... for phase delay 0; 1.2, 1.7, 2.2, ... for phase delay 0.2; 1.4, 1.9, 2.4, ... for phase delay 0.4; 1.6, 2.1, 2.6, ... for phase delay 0.6; and 1.8, 2.3, 2.8, ... for phase delay 0.8. Note that the data points have a step size of 0.1-km IFOV except for a few data points at both ends. Similarly, the step size is 0.05 km for the 0.25-km resolution bands and 0.2 km for the 1-km resolution bands. In general, the smaller detectors have a higher precision in their BBR measurements because of the subsamples. The total number of sample points (N) in the along scan BBR measurements are 200, 100, and 50 for 0.25-, 0.5-, and 1-km bands, respectively.

An example of detector response digital number, dn (dn is SRCA DN with SRCA dark DN, averaged DN of frames 1 and 9, subtracted) versus sample position x_{scan} is illustrated in Fig. 4 using band 3 detector 10. The centroid value of the sample position from the response curve determines the detector position in the along-scan direction [7]

$$\langle x_{\text{scan}}(b,d,m)\rangle = \frac{\sum_{i=1}^{N} x_{\text{scan}}(i) \cdot \text{dn}\,(b,d,m,x_{\text{scan}}(i))}{\sum_{i=1}^{N} \text{dn}\,(b,d,m,x_{\text{scan}}(i))} \tag{2}$$

where $\text{dn}(b,d,m,x_{\text{scan}}(i))$ is the detector's response at position $x_{\text{scan}}(i)$ for a give band (b), detector (d), and mirror side (m), N is the total number of data points, with values of 200, 100, and 50 for the 0.25-, 0.5-, and 1-km resolution bands. Due to the possible existence of a wedge-shaped scan mirror, $\langle x_{\text{scan}}\rangle$ is calculated for each mirror side.

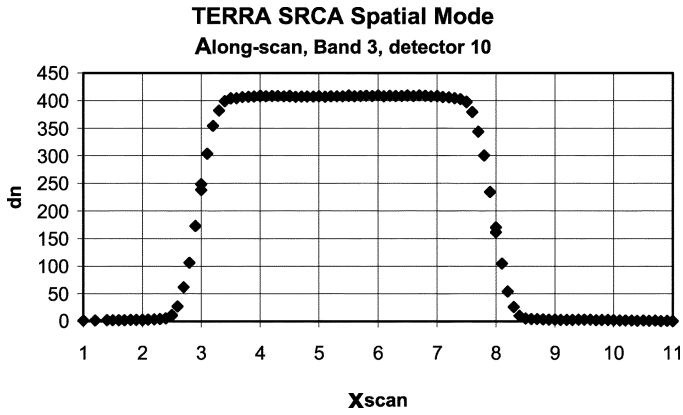

Fig. 4. Detector response in along-scan measurement.

The BBR relative to a reference band (b_o) is the average over both mirror sides given by

$$\Delta x_{\text{scan}}(b,d) = \frac{1}{2}\sum_{m=1}^{2} \left\{\langle x_{\text{scan}}(b,d,m)\rangle - \langle x_{\text{scan}}(b_o,d,m)\rangle\right\}. \tag{3}$$

In the along-scan direction, the BBR can be determined for each detector, sometimes referred to as the detector-to-detector registration (DDR). The final BBR for a band is averaged over its detectors. The precision of the $\langle x_{\text{scan}}\rangle$ or Δx_{scan} is closely related to the precision of the dns. For the thermal emissive bands, one of the potential sources of the measurement uncertainties is the dn variation due to thermal background drift. During the measurement, the phase delay is changed after a certain number of scans (typically 36 scans for each setting). When there is a thermal disturbance, the dns may differ during different phase delays. In our approach we correct the dn differences between phase delays using the dns from frames with full illumination. Electronic crosstalk (observed in the SWIR bands) also causes the dns to change for frames where neighboring bands are illuminated. This effect distorts the response profile and thus impacts the precision of the BBR measurements.

III. Algorithm Using a Fourier Approach for Determining Along-Track BBR

MODIS is a cross track scanning radiometer. Instead of measuring the BBR in the along-track direction for each detector, the MODIS SRCA can only track the BBR from all the detectors in a band as some of the detectors are not illuminated. In the along-track measurement, the four rectangular openings in the along-track reticle [Fig. 3(b)] are equivalent (at nadir) to 2.55 km along-scan and 1.5 km along-track. The along-scan size ensures that two fully illuminated 1-km frames can be obtained for the corresponding detectors. Considering the detector integration time, only frames 4 and 7 of the ten frames of data have dn values unaffected by signal integration transitions. Therefore only the dns from these two frames are utilized in our along-track BBR algorithm. Fig. 5 shows the detectors' responses for a 1-km IFOV band (band 8). Since each detector has a different fraction of illumination by the left and right openings in one scan, its responses or signals are not the same.

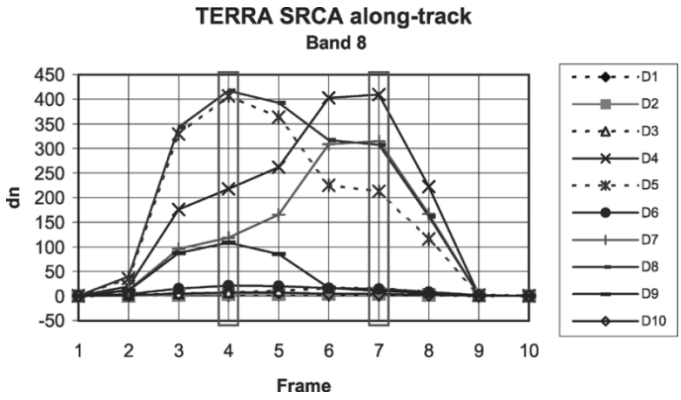

Fig. 5. Detector response under along-track reticle illumination.

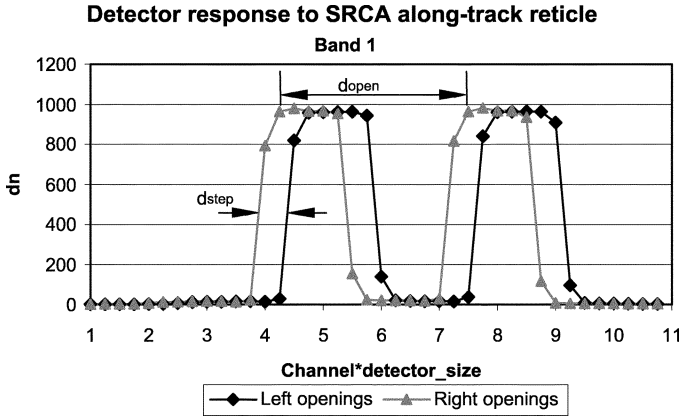

Fig. 6. Detector responses of two groups of openings along-track.

The instrument developer, Raytheon/Santa Barbara Remote Sensing (SBRS) in Goleta, CA, has developed an algorithm which utilizes the opening positions along-track to form a bell-shaped response curve. There are 20 data sample points for the 1-km bands (ten detectors and two frames of data per detector), and 40 and 80 data sample points for the 0.5- and 0.25-km bands. The BBR along-track can thus be determined from the centroid of the bell-shaped response [8].

Fig. 6 shows the detector responses of band 1 with 40 detectors. Two response curves in Fig. 6 correspond to the left and right full opening cases. The distance between the left and the right curves is d_{step}, the step shift between left and right openings in the along-track direction. The distance between two response peaks is equal to d_{open}, the distance between the upper and the lower openings [Fig. 3(b)].

In order to have proper measurement along-track, it is imperative to have a relative calibration (or response normalization) among detectors within a band, since each detector has its own gain. If there is no correction, the dn values in (4) will be weighted by their gain values. In addition, the SRCA output may be nonuniform across the detectors of each band. Vignetting effect may also reduce the dns significantly. Obviously, uncorrected dns will degrade the band position determination. Unlike the along-scan case where the calculation is detector based, along-track BBR calculation combines dns from all detectors in a band.

The relative calibration utilizes the dn from the along-scan measurement. The dn for each detector is determined by averaging over fully illuminated frames. The averaged dn for a band and mirror side $\text{dn}_{\text{av}}(b,m)$ is

$$\text{dn}_{\text{av}}(b,m)_{\text{scan}} = \frac{1}{N_{\text{detector}}(b)} \sum_{d=1}^{N_{\text{detector}}(b)} \text{dn}(b,d,\overline{f},m)_{\text{scan}} \tag{4}$$

where the bar sign implies the average of fully illuminated frames, and $N_{\text{detector}}(b)$ is the number of detectors for the band b. The subscript "scan" indicates that the dn is measured during along-scan calibration.

Therefore, the correction coefficient for a detector $k_{\text{corr}}(b,d,m)$ is

$$k_{\text{corr}}(b,d,m) = \frac{\text{dn}_{\text{av}}(b,m)_{\text{scan}}}{\text{dn}(b,d,\overline{f},m)_{\text{scan}}}. \tag{5}$$

If the dn$'$ is the along-track response before relative calibration, then the after relative calibration dn is given by

$$\text{dn}(b,d,m) = \text{dn}'(b,d,m) \cdot k_{\text{corr}}(b,d,m). \tag{6}$$

Using detector responses with relative calibration, the centroid positions of the left and right response curves $\langle x_{\text{track}}(b,m)\rangle_{\text{L}}$ and $\langle x_{\text{track}}(b,m)\rangle_{\text{R}}$ are calculated by

$$\langle x_{\text{track}}(b,m)\rangle_{\text{L}} = \frac{\sum_{d=1}^{N(b)} x_{\text{track}}(d) \cdot \text{dn}(b,d,f_{\text{L}},m)}{\sum_{d=1}^{N(b)} \text{dn}(b,d,f_{\text{L}},m)} \tag{7}$$

and

$$\langle x_{\text{track}}(b,m)\rangle_{\text{R}} = \frac{\sum_{d=1}^{N(b)} x_{\text{track}}(d) \cdot \text{dn}(b,d,f_{\text{R}},m)}{\sum_{d=1}^{N(b)} \text{dn}(b,d,f_{\text{R}},m)} \tag{8}$$

where $\text{dn}(b,d,f,m)$ is the detector's response at frame f_{L} or f_{R} for a given band (b), detector (d), and mirror side (m), $N(b)$ is the total number of detectors in a band (b). The subscripts L and R are used to indicate the responses from left response curve and right response curve. The values of $x_{\text{track}}(d)$ vary from 1 to 10.75 (40 points) for bands 1 and 2, 1 to 10.5 (20 points) for bands 3–7, and 1 to 10 (10 points) for 1-km bands. There is no subframe number because only dns from the average of all subframes are utilized in this algorithm. The average value of $\langle x_{\text{track}}(b,m)\rangle_{\text{L}}$ and $\langle x_{\text{track}}(b,m)\rangle_{\text{R}}$, $\langle x_{\text{track,avg}}(b,m)\rangle$, when compared with a reference band, determines the relative band centroid shift in the along-track direction.

The disadvantage of using the centroid approach is that the algorithm is not robust. Any bad dns due to noisy or nonfunctional detectors (especially for the illuminated detectors) will significantly impact the band shift value. A Fourier approach was developed [13] to improve the robustness and result consistence according to the data analysis and result comparison. This approach is applied throughout the SRCA spatial measurements.

The BBR shift calculated by the Fourier approach uses the position of the entire profile shown in Fig. 6. The band position along-track is expressed by the phase angle of a periodic

function. Changes in phase uniquely determines the band shift relative to a reference band.

For fast algorithm convergence, we start from the band centroid shift, $\langle x_{\text{track}}(b,m)\rangle - \langle x_{\text{track}}\rangle$, with a bias of φ_{bias} expressed in radians as

$$\varphi_{\text{bias}}(b,m) = \{\langle x_{\text{track,avg}}(b,m)\rangle - \langle x_{\text{track}}\rangle\} \cdot \frac{2\pi}{d_{\text{open}}} + \gamma(b,m) \tag{9}$$

where $\langle x_{\text{track}}\rangle$ is equal to $\langle x_{\text{track}}(b,m)\rangle$ when the band has no shift in the along-track direction.

The value of $\langle x_{\text{track}}\rangle$ depends on the reticle position relative to the FPA. The phase angle $\gamma(b,m)$ is initialed as zero. Again, we treat each mirror side separately. Therefore, the phase angles corresponding to the two response curves for each detector can be calculated by

$$\theta_{\text{L}}(b,d,m) = [x_{\text{track}}(d) - \langle x_{\text{track}}\rangle - 0.5 \cdot d_{\text{step}}] \cdot \frac{2\pi}{d_{\text{open}}} - \varphi_{\text{bias}}(b,m) \tag{10}$$

$$\theta_{\text{R}}(b,d,m) = [x_{\text{track}}(d) - \langle x_{\text{track}}\rangle + 0.5 \cdot d_{\text{step}}] \cdot \frac{2\pi}{d_{\text{open}}} - \varphi_{\text{bias}}(b,m) \tag{11}$$

where $x_{\text{track}}(d)$ is the same as in (7) and (8). The periodic function is considered only in the range from -2π to 2π. All the phase angles beyond this range will be set to zero. The Fourier sine and cosine components can therefore be expressed by [14]

$$S_x(b,m) = \sum_{d=1}^{N(d)} \{\text{dn}(b,d,f_{\text{L}},m) \cdot \sin\theta_{\text{L}}(b,d,m) + \text{dn}(b,d,f_{\text{R}},m) \cdot \sin\theta_{\text{R}}(b,d,m)\} \tag{12}$$

and

$$S_y(b,m) = \sum_{d=1}^{N(d)} \{\text{dn}(b,d,f_{\text{L}},m) \cdot \cos\theta_{\text{L}}(b,d,m) + \text{dn}(b,d,f_{\text{R}},m) \cdot \cos\theta_{\text{R}}(b,d,m)\}. \tag{13}$$

Thus the phase angle is calculated

$$\gamma(b,m) = a\tan\left(S_x(b,m), S_y(b,m)\right). \tag{14}$$

The phase angle is a correction to $\varphi_{\text{bias}}(b,m)$ in (9). The iteration continues until the phase angle correction is converged to a preset small number. The final band shift relative to its ideal position along-track is the average of the shifts from both mirror sides

$$\Delta x_{\text{track}}(b) = \frac{1}{2}\sum_{m=1}^{2} \frac{\varphi_{\text{bias}}(b,m)}{2\pi} \cdot d_{\text{open}}. \tag{15}$$

The use of a periodic function to approximate the actual response curve may cause some theoretical uncertainty. This estimated uncertainty is about 1 m over a shift range of ± 0.1 km along-track. Therefore the Fourier approach is acceptable for the along-track BBR calculations.

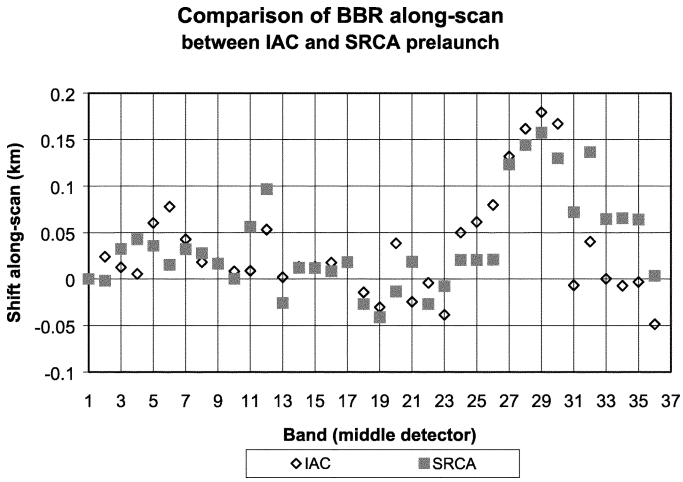

Fig. 7. BBR along-scan, comparison between IAC and SRCA.

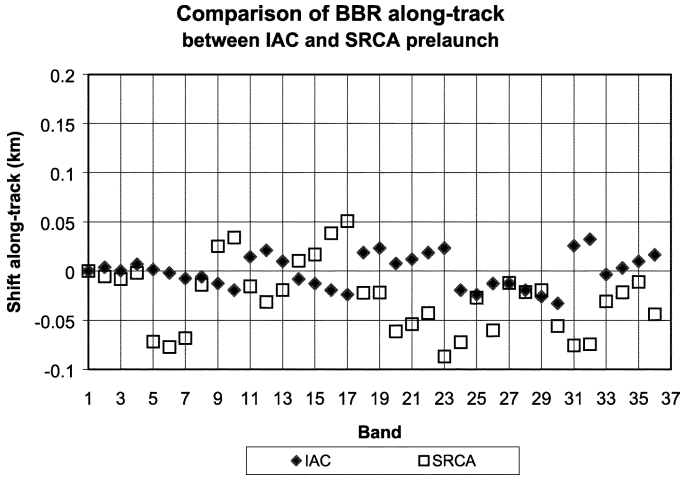

Fig. 8. BBR along-track, comparison between IAC and SRCA.

IV. BBR Measurements

MODIS specification requests that the BBR between any bands be within 0.2 km. This means the BBR for all 36 bands should be located in a belt in width of 0.2 km wide in both along-scan and along-track directions.

A. Prelaunch Calibration

The MODIS BBR was measured prelaunch at SBRS using the integration and alignment collimator (IAC). The IAC output uniformly fills the MODIS aperture. In the along-scan measurement, a narrow slit is scanned across the MODIS detectors. Fine phase delays with a step size of 0.1 km are applied to increase the measurement precision. The centroid value of each detector along-scan is calculated from the detector's response profile. When the BBR in the along-track direction is measured, a reticle with three inclined narrow slits is utilized. The inclination angle is such that each slit moves 1-km IFOV along-track as the reticle moves 12-km IFOV along-scan. Thus, only three 1-km IFOV detectors can have signals that produce a dn versus data frame

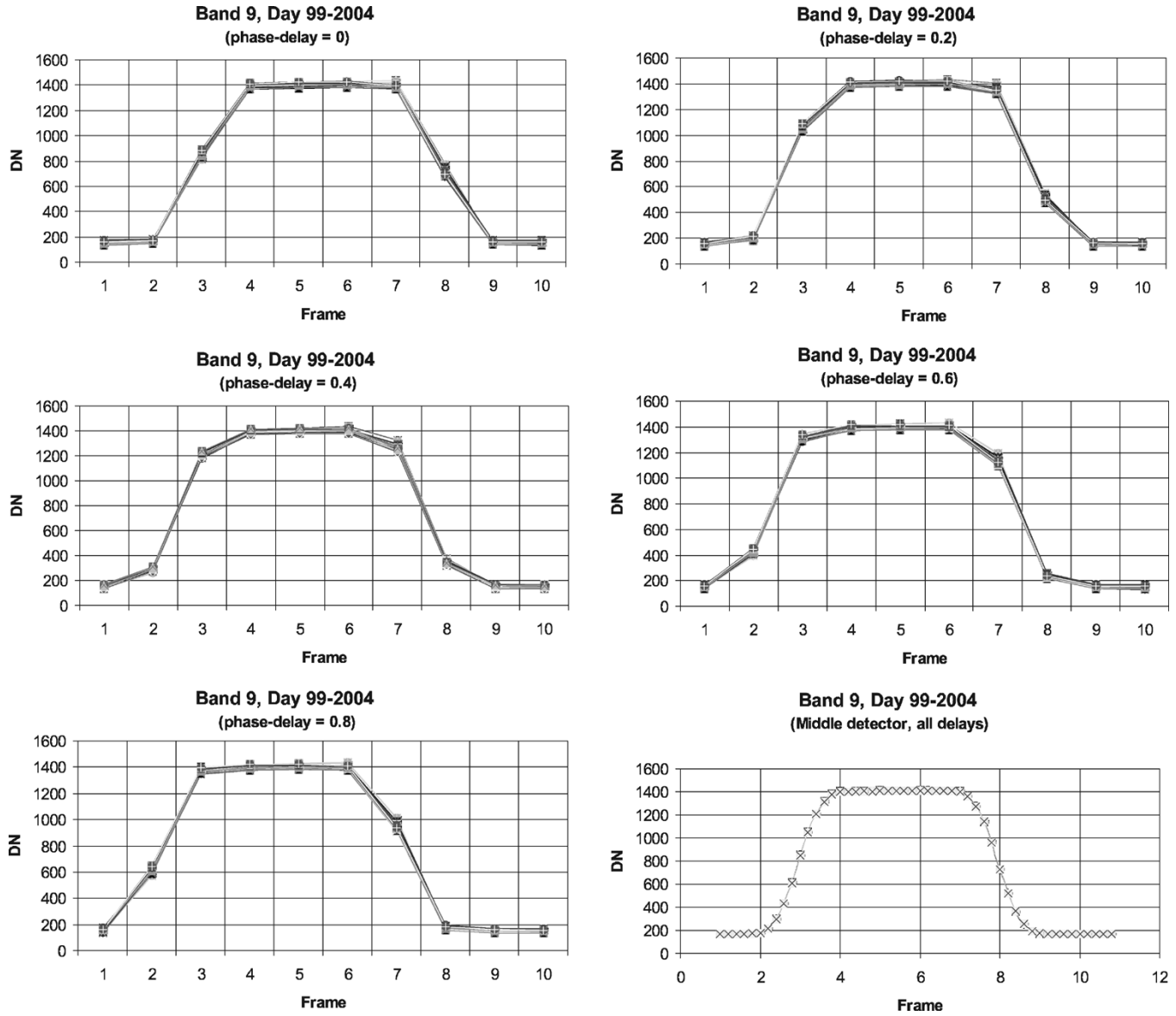

Fig. 9. SRCA along-scan signal at different phase delay and their combination.

profile. The average of these three centroid values determines the BBR along-track. The IAC results provide the prelaunch BBR for the instrument.

During prelaunch spatial characterization, the SRCA was also operated to measure the BBR in the same environment and at nearly the same time as the IAC. The difference (or offset) in BBR between the IAC and the SRCA is used as a correction term for the SRCA measurements and is assumed to remain unchanged throughout on-orbit operations.

During on-orbit calibration and characterization, the SRCA is periodically operated in spatial mode to check the BBR changes over time. The on-orbit BBR values at time t are equal to the on-orbit SRCA BBR results at time t plus the prelaunch offset between IAC and SRCA at t_o

$$\begin{aligned}\mathrm{BBR}_{\mathrm{scan}}(b,d,t) = {} & \mathrm{BBR}_{\mathrm{scan,SRCA}}(b,d,t) \\ & + \mathrm{BBR}_{\mathrm{scan,IAC}}(b,d,t_o) \\ & - \mathrm{BBR}_{\mathrm{scan,SRCA}}(b,d,t_o) \qquad (16)\end{aligned}$$

$$\begin{aligned}\mathrm{BBR}_{\mathrm{track}}(b,t) = {} & \mathrm{BBR}_{\mathrm{track,SRCA}}(b,t) \\ & + \mathrm{BBR}_{\mathrm{track,IAC}}(b,t_o) \\ & - \mathrm{BBR}_{\mathrm{track,SRCA}}(b,t_o). \qquad (17)\end{aligned}$$

When the SRCA was first mounted in the MODIS, the alignment between the MODIS FPAs and the SRCA was carefully adjusted. However, misalignment may have occurred during testing and during spacecraft launch. To minimize errors due to misalignment between MODIS and the SRCA, the BBR is relative to a reference band. Band 1 is selected for this purpose for the following reasons: 1) it has the highest spatial resolution and the highest precision in BBR the measurements; 2) it is located near the sensor's optical axis; and 3) its response is high under the SRCA illumination. To determine the geolocation of MODIS images, the ground footprint of band 1 is carefully determined using ground control points worldwide [15], and all other band/detector footprints are determined using the BBR values relative to band 1.

The Terra MODIS prelaunch BBR was initially measured in ambient. In this test, the SMIR and LWIR focal planes were cooled by a bench test cooler (BTC). Unfortunately, the SNRs were too low for bands 5, 6, 20, and 22. The BBR values for these bands have been estimated from their neighboring bands and verified by the SRCA results from thermal vacuum (TV) tests. Figs. 7 and 8 illustrate the BBR measured by the IAC and the SRCA in both the along-scan and along-track directions. It shows that the BBR is slightly out of specification for bands 28, 29, and 30 along-scan.

The BBR results in Figs. 7 and 8 indicate that there are appreciable differences between the IAC and the SRCA for some bands along-scan. One possible reason for this is that the SRCA only partially fills the MODIS aperture. Differences in slit width between the two devices and crosstalk between some bands can also cause differences. Nonuniform thermal (temperature) distribution along the SRCA reticle could also introduce bias in the thermal bands.

The measurement of band centroids along-track has relatively large IAC/SRCA differences. This may be due to the use of three measured detector positions in the IAC measurements, whereas the SRCA uses signals from all detectors. It is not critical to match the two measurements as long as the SRCA measurements remain stable and repeatable. The IAC provides absolute BBR values, while the SRCA detects changes from test to test.

B. BBR Tracking On-Orbit

The SRCA was operated in the spatial mode during prelaunch TV testing at cold, nominal, and hot instrument temperature plateaus and was retested at the spacecraft integration stage at similar instrument temperatures to monitor the changes in BBR prior to launch. After the first 100 days of on-orbit operation, the instrument stabilized. Since then, the SRCA has been used periodically to monitor the BBR variation over time [9].

Fig. 9 shows examples of MODIS band 9 detector responses (dns) during SRCA along-scan spatial characterization on day 2 004 099. The DNs for all detectors and scans are overplotted in Fig. 9(a)–(e) for five different phase delays (0, 0.2, 0.4, 0.6, and 0.8) to illustrate the scan-to-scan repeatability and response uniformity of detectors in a band. Fig. 9(f) is the along-scan response derived by combining data points from all phase delays for the band 9 middle detector. The high precision of SRCA spatial characterization is illustrated via the consistency in the long-term trending. Table I provides a comparison of detector-to-detector registration (DDR) between prelaunch (nominal temperature plateau) and on-orbit (day 2 004 099). The data show that the DDR patterns (DDR versus detector number) are very consistent for the two datasets that were taken seven years apart. The BBR difference calculated for mirror sides 1 and 2 is less than 0.003 km, illustrating the measurement repeatability. On the other hand, the mirror side differences in BBR without normalized to band 1 can be utilized in estimating the inclination angle between the two surfaces of the mirror. Based on the available data, the mirror side wedge angles are less than 2.41 $\pm$ 0.21 arcsec. along-scan and 2.87 $\pm$ 0.16 arcsec. along-track.

Figs. 10 and 11 summarize the spatial characterization results from four years of Terra MODIS (PFM) BBR in both the along-scan and along-track directions. The x axis is days from January 1, 2000. The prelaunch nominal plateau results are used as the reference for the on-orbit trending. The four separate plots correspond to the four MODIS FPAs: VIS, NIR, SMIR, and LWIR. The band numbers, in sequence of band location on the FPAs, are given in the legends. There are four vertical lines in these plots. The first two correspond to when the electronics configuration was changed from side A to side B on day 2 000 304 and then changed back from side B to side A on day 2 001 083. As one would expect, the electronic changes had no impact on the BBR.

TABLE I
COMPARISONS OF MODIS BAND 3 DDR BETWEEN PRELAUNCH TV TEST AT NOMINAL (NOM) TEMPERATURE PLATEAU AND ON-ORBIT MEASUREMENT ON DAY 2 004 099

Band	Detector	Nom_TV		Day 2004099		Nom_TV	2004099
		MS_1	MS_2	MS_1	MS_2	MS_2 - MS_1	
3	1	-0.0355	-0.0352	-0.0062	-0.0084	0.0003	-0.0022
3	2	-0.0353	-0.0358	-0.0051	-0.0082	-0.0005	-0.0031
3	3	-0.0291	-0.0287	-0.0004	-0.0033	0.0004	-0.0029
3	4	-0.0306	-0.0312	-0.0013	-0.0032	-0.0006	-0.0019
3	5	-0.0306	-0.0302	-0.0017	-0.0040	0.0004	-0.0023
3	6	-0.0300	-0.0289	-0.0008	-0.0028	0.0011	-0.0020
3	7	-0.0334	-0.0333	-0.0049	-0.0063	0.0001	-0.0014
3	8	-0.0298	-0.0283	-0.0001	-0.0033	0.0015	-0.0031
3	9	-0.0318	-0.0325	-0.0026	-0.0046	-0.0007	-0.0020
3	10	-0.0355	-0.0346	-0.0045	-0.0070	0.0009	-0.0025
3	11	-0.0337	-0.0337	-0.0038	-0.0062	0.0000	-0.0024
3	12	-0.0335	-0.0324	-0.0028	-0.0043	0.0011	-0.0015
3	13	-0.0344	-0.0340	-0.0033	-0.0055	0.0004	-0.0022
3	14	-0.0301	-0.0290	0.0010	-0.0013	0.0011	-0.0023
3	15	-0.0298	-0.0288	0.0011	-0.0023	0.0010	-0.0033
3	16	-0.0273	-0.0254	0.0038	0.0008	0.0019	-0.0030
3	17	-0.0241	-0.0239	0.0057	0.0032	0.0002	-0.0025
3	18	-0.0223	-0.0215	0.0088	0.0065	0.0008	-0.0023
3	19	-0.0225	-0.0225	0.0074	0.0042	0.0000	-0.0032
3	20	-0.0259	-0.0259	0.0047	0.0025	0.0000	-0.0022

The other two vertical lines mark the time period in which the SRCA measurements were impacted by sunlight coming from the Terra MODIS solar diffuser. Typically, the SD door opens only during the SD calibration time frame, and the SRCA is operated during earth nighttime part of the orbit. Due to an SD door operation anomaly on day 2003183, a decision was made to keep the SD door in the open position. Now, the SD is illuminated every orbit because of the SD door position. Because of this, the MODIS signal from the SRCA is contaminated by sunlight from the SD for a small period of time (the SD is illuminated before the satellite enters the earth daytime part of the orbit). In order to avoid this contamination, the SRCA spatial characterization is run 3 min earlier starting from day 2 003 330 to allow the SRCA measurement to finish before the sun illuminates the SD.

The along-scan BBR for the VIS FPA has a small but noticable periodic oscillation pattern with amplitude of about 20 m (ground footprint at nadir). As will be discussed later, the oscillation matches closely to the instrument temperature variation. The NIR FPA has minimal variation because the BBR variation is relative to band 1 located on the NIR FPA. The SMIR FPA has unique variation at the beginning of the mission. This is because during the first 100 days, a series of changes were made to the SMIR focal plane detector biases in an attempt to reduce the identified electronic crosstalk. After the detector parameter settings were fixed, the SMIR BBR became very stable. For the LWIR FPA, the BBR shifted to a different position in the first 100 days and since then has been very stable. The current

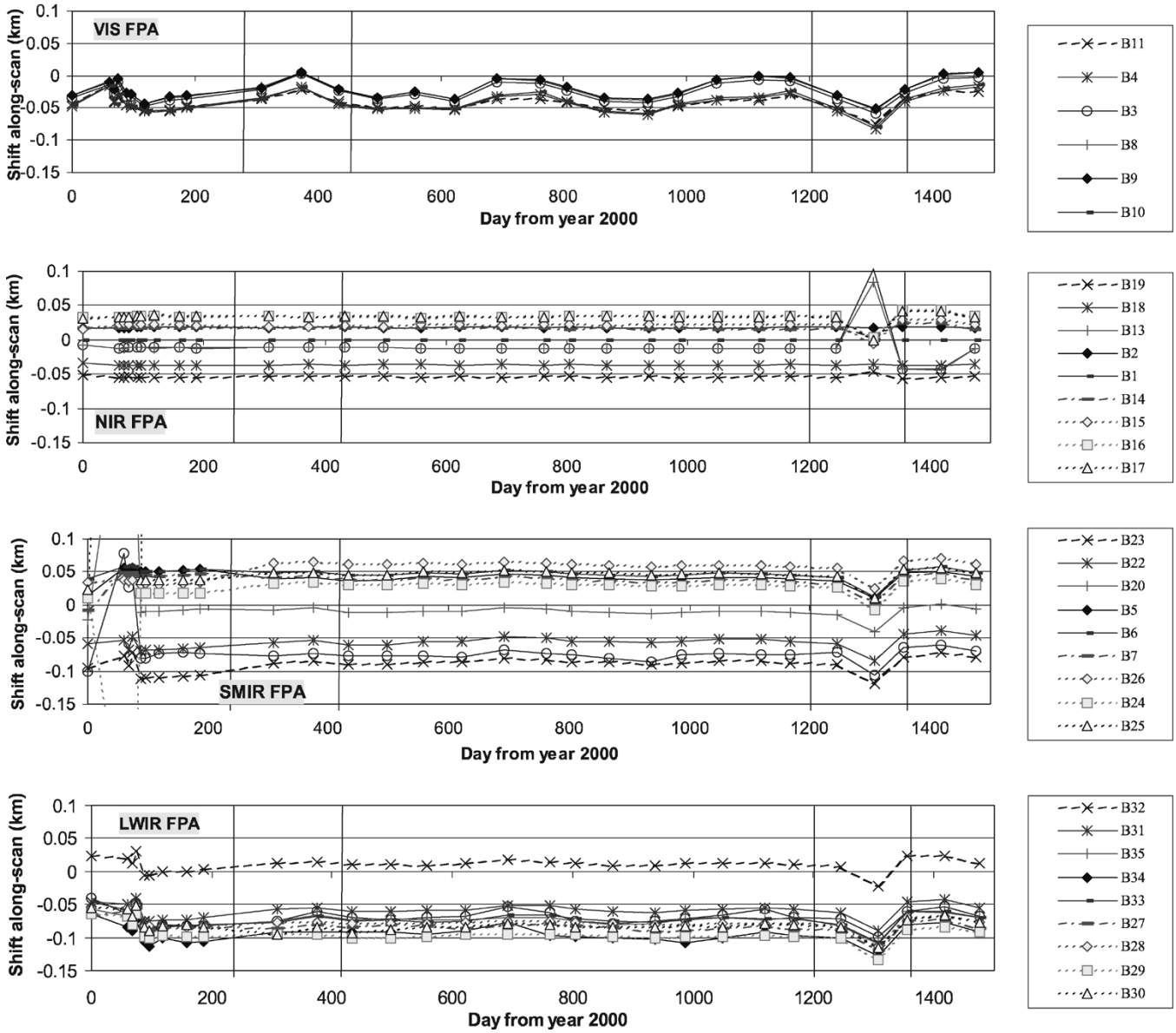

Fig. 10. BBR along-scan trending on-orbit.

BBR along-scan values are less than 0.16 km after adding the prelaunch offset, thus meeting the specification.

Like the along-scan BBR trending, the results from the along-track BBR trending show a small shift during initial on-orbit operations for the VIS FPA, and since then, it has remained fairly constant. The NIR FPA has no problems with stability as one would expect, since the BBR is normalized to band 1 on the NIR FPA. Both the SMIR and LWIR FPAs moved to different positions shortly after launch and have since remained stable. The current BBR along-track values are all within specification, except for the BBR between bands 26 and 30 at 0.23 km, which is 30 m out of the specification. Table II summarizes the most recent BBR values for all 36 spectral bands in both the along-scan and along-track directions.

It is worth to mentioning that the SRCA spatial mode is also a useful tool to monitor the modulation transfer function (MTF). The along-scan measurement is equivalent to using knife-edge scans across the detectors. The edge of the reticle located at the focus of the SRCA collimator is imaged onto the FPAs, producing a sharp line perpendicular to scan direction. The derivative of the knife-edge response is the line-spread function (LSF) from which system MTF can be evaluated. Multiple phase delays further enhance the measurement precision.

V. BBR Variation Versus Instrument Temperature

As shown in Fig. 10, the VIS FPA along-scan BBR trending clearly displays an annual oscillation. Analysis of instrument on-orbit telemetry during the SRCA measurements indicates that this oscillation is correlated to the instrument temperature variations that result from the annual sun–satellite distance variation. The MODIS instrument temperature is measured by a thermistor located near the SMIR objective lens. Fig. 12 is the BBR trending on-orbit for band 9, all ten detectors. The BBR variation for all detectors are essentially the same. A trending line is drawn for detector 5.

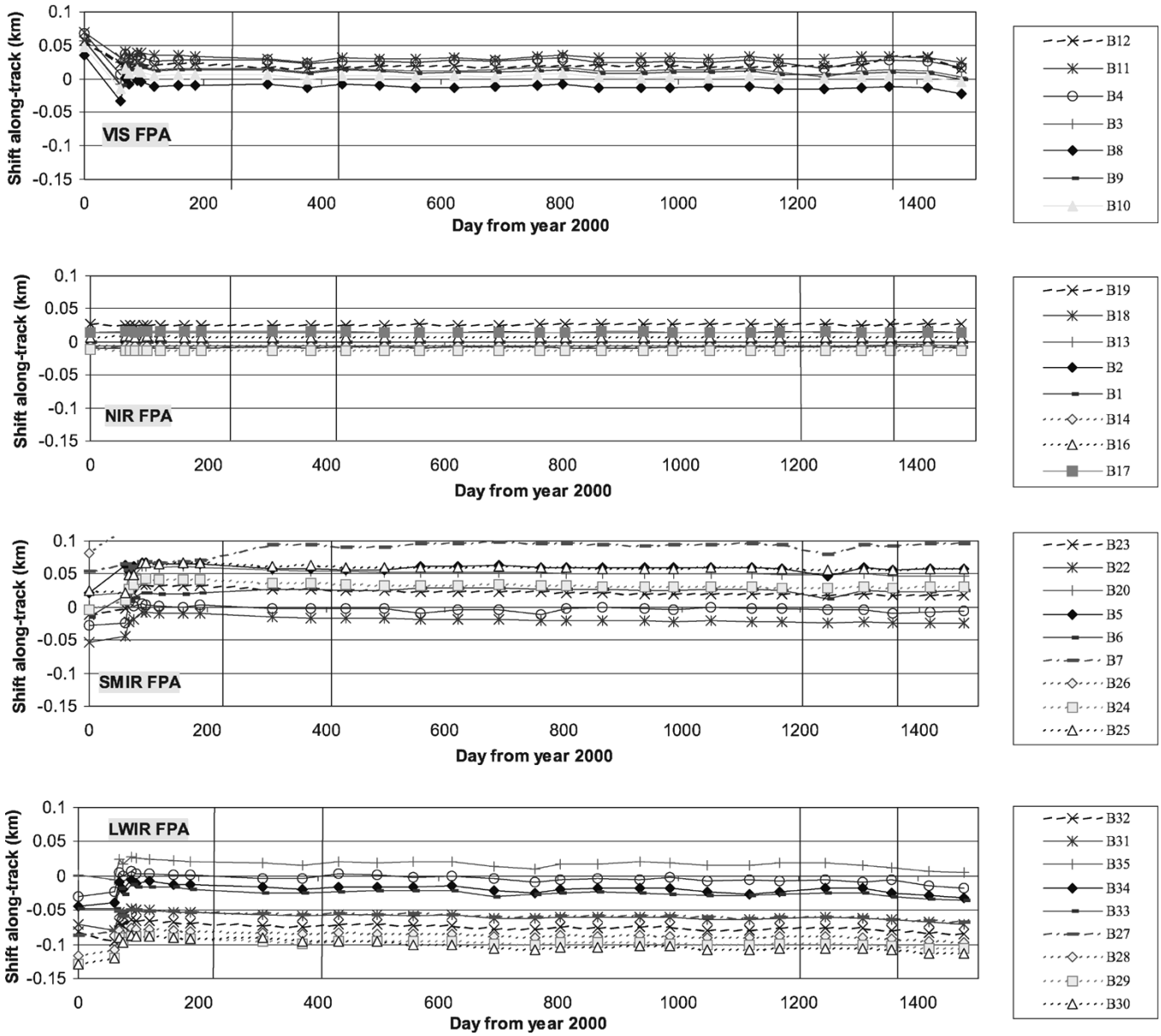

Fig. 11. BBR along-track trending on-orbit.

TABLE II
EXAMPLE OF ON-ORBIT BBR RESULTS (DAY 2 004 099)

Band	Along-scan	Along-track	Band	Along-scan	Along-track
1	0	0	19	-0.0545	0.0263
2	0.0186	-0.0002	20	-0.0127	0.0476
3	-0.0058	0.0015	21	-0.0992	-0.0031
4	-0.0334	0.0175	22	-0.0536	-0.0246
5	0.0379	0.0564	23	-0.0873	0.0169
6	0.0425	0.0232	24	0.0263	0.0288
7	0.0335	0.0957	25	0.0432	0.0567
8	-0.0003	-0.0246	26	0.0567	**0.1169**
9	0.0018	-0.0021	27	-0.0883	-0.0607
10	-0.0294	-0.006	28	-0.0813	-0.0899
11	-0.0332	0.0269	29	-0.1001	-0.0998
12	0.0039	0.0175	30	-0.0868	**-0.1068**
13	-0.0134	-0.0052	31	-0.0676	-0.062
14	0.0157	-0.0063	32	-0.0008	-0.0762
15	0.0222	-0.0132	33	-0.0822	-0.0286
16	0.0356	0.0071	34	-0.1045	-0.0207
17	0.0313	0.0153	35	-0.087	0.0134
18	-0.0384	0.0147	36	-0.0844	-0.0063

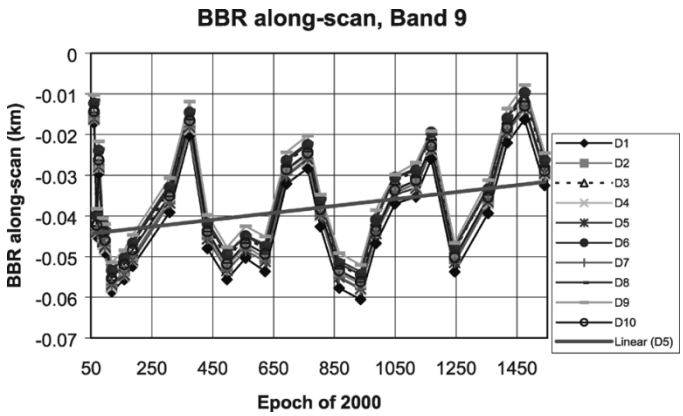

Fig. 12. BBR along-scan trending for band 9.

In Fig. 13, the MODIS instrument temperature trending is provided for the same time period. We can see that the instru-

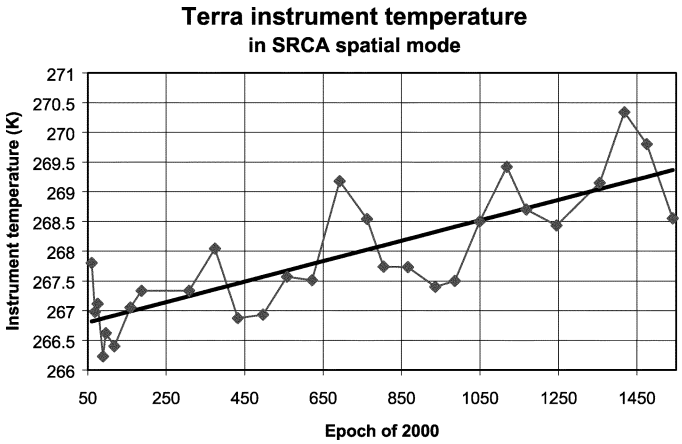

Fig. 13. Instrument temperature variation trending in SRCA spatial mode.

ment temperature change contains two components: one is slow increase over time, and the other is an annual variation; both correlate with the VIS BBR trending pattern very well.

The FPA averaged temperature coefficients along-scan, expressed in meters per degree, are as follows: 16.7 ± 3.2 m/K (VIS), 0.0 ± 0.3 m/K (NIR), 3.6 ± 1.0 m/K (SMIR), and 4.0 ± 1.6 m/K (LWIR). The along-track coefficients are -0.6 ± 0.6 m/K (VIS), 0.0 ± 0.1 m/K (NIR), 1.0 ± 1.2 m/K (SMIR), and -2.8 ± 0.9 m/K (LWIR). Except for the VIS along-scan direction, the temperature coefficients are very small. In deriving the coefficients, some of the data points were excluded, such as those during early instrument configuration adjustment and bad data points due to SD door-open impact. The bands located at the FPA edges with out-of-family data were also excluded.

VI. Conclusion

The SRCA measures the band-to-band registration changes from prelaunch to on-orbit so that the on-orbit BBR can be tracked after correcting for the bias between the IAC and the SRCA. The BBR algorithms for along-scan and along-track measurements have been presented. The Fourier approach for the along-track BBR calculation improves the measurements' robustness. The prelaunch tests show that the Terra MODIS BBR meets the specification with only a few exceptions along-scan. The BBR has changed very slightly on-orbit. Four years after launch, the BBR is still in specification (0.2 km) along-scan, but 30 m larger than the specification along-track (band 26 to band 30 only). The BBR varies with instrument temperature. The VIS FPA has the largest temperature coefficients. The along-scan FPA averaged temperature coefficients are 16.7 ± 3.2 m/K (VIS), 0.0 ± 0.3 m/K (NIR), 3.6 ± 1.0 m/K (SMIR), and 4.0 ± 1.6 m/K (LWIR). The along-track coefficients are -0.6 ± 0.6 m/K (VIS), 0.0 ± 0.1 m/K (NIR), 1.0 ± 1.2 m/K (SMIR), and -2.8 ± 0.9 m/K (LWIR).

Acknowledgment

The authors wish to thank their Raytheon SBRS colleagues for sharing expertise and knowledge, for their continued technical support, and for invaluable discussions.

References

[1] W. L. Barnes, T. S. Pagano, and V. V. Salomonson, "Pre-launch characteristics of the Moderate Resolution Imaging Spectroradiometer (MODIS) on EOS AM-1," *IEEE Trans. Geosci. Remote Sens.*, vol. 36, no. 4, pp. 1088–1100, Jul. 1998.

[2] V. V. Salomonson, W. L. Barnes, X. Xiong, S. Kempler, and E. Masuoka, "An overview of the Earth Observing System MODIS instrument and associated data systems performance," in *Proc. IGARSS*, 2002.

[3] W. L. Barnes, X. Xiong, and V. V. Salomonson, "Status of Terra MODIS and Aqua MODIS," *J. Adv. Space Res.*, vol. 32, no. 11, pp. 2099–2106, 2003.

[4] X. Xiong, K. Chiang, J. Esposito, B. Guenther, and W. L. Barnes, "MODIS on-orbit calibration and characterization," *Metrologia 40*, pp. 89–92, 2003.

[5] X. Xiong, K. Chiang, B. Guenther, and W. I. Barnes, "MODIS thermal emissive bands calibration algorithm and on-orbit performance," *Proc. SPIE*, vol. 4891, pp. 392–401, 2003.

[6] X. Xiong, J. Sun, J. Esposito, B. Guenther, and W. L. Barnes, "MODIS reflective solar bands calibration algorithm and on-orbit performance," *Proc. SPIE*, vol. 4891, pp. 95–104, 2003.

[7] H. Montgomery, N. Che, and J. Bowser, "Determination of the spatial characteristic by using the spectro-radiometric calibration assembly (SRCA) of MODIS (part I. Along-scan)," *Proc. SPIE*, vol. 3439, pp. 226–237, 1998.

[8] ——, "Determination of the spatial characteristic by using the spectro-radiometric calibration assembly (SRCA) of MODIS (part II. Along-track)," *Proc. SPIE*, vol. 3439, pp. 238–246, 1998.

[9] X. Xiong and N. Che, "On-orbit spatial characterizations for Terra MODIS," *Proc. SPIE*, vol. 4814, pp. 347–357, 2002.

[10] H. Montgomery, N. Che, K. Parker, and J. Bowser, "The algorithm for MODIS wavelength on-orbit calibration bands using the SRCA," *IEEE Trans. Geosci. Remote Sens.*, vol. 38, no. 2, pp. 877–884, Mar. 2000.

[11] N. Che, X. Xiong, and W. L. Barnes, "On-orbit spectral characterization of the Terra MODIS reflective solar bands," *Proc. SPIE*, vol. 5151, pp. 367–374, 2003.

[12] X. Xiong, A. Wu, J. Esposito, J. Sun, N. Che, B. Guenther, and W. L. Barnes, "Trending results of Terra MODIS optics on-orbit degradation," *Proc. SPIE*, vol. 4814, pp. 337–346, 2002.

[13] J. Bauer, private communication, Aug. 30, 1999.

[14] W. H. Press, S. A. Teukolsky, W. T. Vetterling, and B. P. Flannery, *Numerical Recipes in Fortran 77*, 2nd ed. Cambridge, U.K.: Cambridge Univ. Press, 1992, vol. 1, pp. 494–498.

[15] R. Wolfe, M. Nishihama, A. Fleig, J. Kuyper, D. Roy, J. Storey, and F. Patt, "Achieving sub-pixel geolocation accuracy in support of MODIS land science," *Remote Sens. Environ.*, vol. 83, pp. 31–49, 2002.

Xiaoxiong Xiong received the B.S. degree in optical engineering from the Beijing Institute of Technology, Beijing, China, and the Ph.D. degree in physics from the University of Maryland, College Park.

He is currently an Optical Physicist with the National Aeronautics and Space Administration (NASA) Goddard Space Flight Center, Greenbelt, MD, currently working on the EOS Terra/Aqua MODIS project and NPOESS/VIIRS instrument calibration and characterization. Before he joined NASA's instrument calibration program, he had also worked in the fields of nonlinear optics, laser/atomic spectroscopy, and mass spectrometry in private industry and with the National Institute of Standards and Technology.

Nianzeng Che has been a member of the MODIS Calibration Support Team (MCST) for over ten years. He became an Associate Professor with the Beijing Institute of Technology, Beijing, China, in 1985. He has been working in various fields of remote sensing (field and laboratory measurements, instrument calibration, image processing, data application, and analysis) since 1982. He has been with the Optical Science Center, University of Arizona; U.S. Department of Agriculture's Beltsville Agriculture Research Center; Swales Aerospace Company on the Thematic Mapper, SPOT, AVHRR, and MODIS; and currently is with Science Systems and Application, Inc., Lanham, MD, working on MODIS projects.

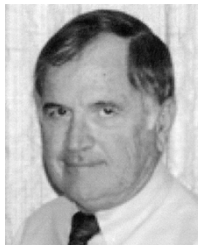

William Barnes received the B.S. and M.S. degrees from the University of North Texas, Denton, in 1960 and 1961, respectively, and the Ph.D. degree from Florida State University, Tallahassee, in 1970, all in physics.

He is currently a Senior Research Scientist with the Joint Center for Earth Systems Technology, University of Maryland Baltimore County, Baltimore, and an Emeritus Research Scientist with the Earth Sciences Directorate, NASA Goddard Space Flight Center, Greenbelt, MD. He has served as the MODIS Sensor Scientist and as a member of the MODIS Science Team for more than 12 years. He has led the MODIS Characterization Support Team for two years and has over 30 years experience in the development and radiometric calibration of earth-observing imaging radiometers.